

Supporting Information

I. Experimental section

General. Nickel nitrate hexahydrate (99.99% metals basis), Ammonium molybdate tetrahydrate (99.9%), Ruthenium(IV) oxide (RuO_2 , 99.99%), Pt(5%)-C, benzyl alcohol (> 99.9%), 2-methylbenzyl alcohol (2-m-BA, > 97%), 3-methylbenzyl alcohol (3-m-BA, > 98%), oleylamine (80-90%), potassium hydroxide (99.9%) and magnesium sulfate (MgSO_4 , > 98%) were purchased from aladdin and were used as received. Nickel foam (NF) with a thickness of 0.1 cm and Titanium foil (99.7%) with a thickness of 0.25 mm were purchased from Beijing General Research Institute for Nonferrous Metals. $\text{Mo}(\text{CO})_6$ (98%) and 1-Octadecene (90%) were purchased from Alfa Aesar. Nickel(II) acetylacetonate ($\text{Ni}(\text{acac})_2$, 98%) was obtained from Adamas-Beta.

Physical Measurements. Powder X-ray diffraction (XRD) patterns were recorded on a X-ray diffractometer with Cu $\text{K}\alpha$ radiation (Bruker AXS, D8 Advance). Scanning electron microscopy (SEM) was carried out on a Hitachi apparatus (S-4800) working at an acceleration voltage of 5 kV. Transmission electron microscopy (TEM) and elemental mapping analysis were performed on Tecnai G2 20 S-TWIN operated at 200 kV. X-ray photoelectron spectroscopy (XPS) was measured with Al $\text{K}\alpha$ X-ray radiation (Thermo Fisher, ESCALAB 250XI). The organic compounds in the electrolyte were analyzed by GC7890F equipped with a flame ionization detector and a GC (Thermo Trace 1300)-MS (Thermo ISQ QD) system after neutralization.

Pretreatment of NF. The NF was first cut into small pieces (2.0 cm x 3.0 cm), and then the small-sized nickel foams were added into a HCl solution (3.0 M). After being sonicated for 10 min, the NFs were removed from the mixture and further washed several times with ethanol and de-ionized water. The treated NFs were dried under vacuum at 60 °C overnight.

Growth of NiMoO_4 Microrod arrays on NF (NiMoO_4/NF). The growth of NiMoO_4 microrod arrays on the treated NF was carried out by a reported method with slight modifications.^{1,2} In brief, a precursor solution was first prepared by dissolving nickel nitrate hexahydrate (0.3492 g) and ammonium molybdate tetrahydrate (0.3705 g) into de-ionized water (30 mL). Thereafter, the precursor solution, together with a piece of the treated NF (2.0 cm x 3.0 cm) was transferred into a 45-mL Teflon-lined autoclave, and the autoclave was heated at 160 °C for 4 h. After cooling to room temperature, the resulting nickel foam was removed, washed several times with ethanol and dried for further use.

Growth of Mo-Ni alloy nanoparticles on MoO_2/NF . The growth of Mo-Ni alloy nanoparticles on the surface of the substrate was performed by direct reduction of NiMoO_4/NF under H_2 (5 %)/Ar atmosphere at high temperatures. Typically, the as-treated NiMoO_4/NF was placed into a tube furnace and then heated at 500 °C for 2 h under the reductive atmosphere. Notably, the reduction treatment should be carried out for 2 times to enable the completed reduction of the precursor material of NiMoO_4 , and the resulting NF was inverted in the second treatment.

Evaluation of mass loading of Mo-Ni alloy nanoparticles on the surface of MoO_2 microrods. To exclude the impact of Ni foam in the evaluation of mass loading of Mo-Ni alloy nanoparticles on the surface of MoO_2 microrods, NiMoO_4 microrods were grown on the surface of carbon cloth (CC). The method is essentially the same to that for the synthesis of NiMoO_4/NF except that a piece of carbon cloth (2.0 cm x 3.0 cm) is used to replace the Ni foam substrate. The as-prepared NiMoO_4/CC was further treated at 500 °C for 2 h (two times) under H_2 (5 %)/Ar atmosphere to afford $\text{Mo-Ni}/\text{MoO}_2/\text{CC}$. The resulting $\text{Mo-Ni}/\text{MoO}_2/\text{CC}$ was etched in H_2SO_4 to remove Mo-Ni alloy nanoparticles. The mass loading was obtained based on the weight difference of the $\text{Mo-Ni}/\text{MoO}_2/\text{CC}$ substrate before and after the etching treatment.

Preparation of Mo_{0.6}Ni_{0.4}/Ti. Preparation of Mo_{0.6}Ni_{0.4}/Ti. The alloy nanoparticles of Mo_{0.6}Ni_{0.4} were synthesized by thermal decomposition of Mo(CO)₆ and Ni(acac)₂ in the presence of oleylamine and 1-octadecene at high temperatures.³ The purified Mo_{0.6}Ni_{0.4} alloy nanoparticles were redispersed in cyclohexane to form a homogeneous colloid solution (5 mL). For preparation of Mo_{0.6}Ni_{0.4}/Ti, the as-prepared Mo-Ni alloy nanoparticles (25 μ L, 10 mg/mL) were placed on one side of the treated Ti foil. Thereafter, the resultant Ni-Mo alloy nanoparticle-coated Ti foil was treated under a reducing atmosphere (H₂ (5%)/Ar) at 450°C for 2 h to remove the organic ligand.

Preparation of RuO₂/NF. The electrode was prepared by a reported method.² In a typical experiment, RuO₂ (5 mg, 99.99%) was first dispersed in ethanol (2.0 mL) by sonication for 10 min. Next, a drop of the resulting homogeneous dispersion (1.0 mL) was placed on a pre-treated NF (1 cm \times 1 cm). The catalyst of RuO₂ loaded on NF was fixed at 2.5 mg cm⁻².

Preparation of Pt (5 %)-C/NF. The synthetic procedure for Pt(5 %)-C/NF was identical to that for RuO₂/NF except that Pt(5 %)-C was used to replace RuO₂ in the preparation. The loading of Pt(5 %)-C was also set at 2.5 mg cm⁻².

Evaluation of unreacted BA, formed benzaldehyde and benzoic acid from the electrolyte. After electrochemical reactions, a mixture of KOH (20 mL) was removed from the anode chamber to which HCl was added. Upon neutralization, dichloromethane (10 mL) was added into the mixture to extract the organic compounds. The extraction procedures were repeated for 3 times. The organic layers were combined together, which was dried by MgSO₄. The organic mixture was obtained via vacuum evaporation, and then dissolved in acetic ether (2 mL) for gas chromatography-mass spectrometry measurement.

OER, anodic oxidation of BA and HER measurements. These measurements were performed with a H-type three-compartment cell using a CHI 770e (CH Instruments, Chenhua, Shanghai) electrochemical workstation. The anode and cathode chambers were separated by a Nafion membrane. The as-prepared Mo-Ni alloy nanoparticle catalyst (1 cm \times 1 cm) was used as a bifunctional electrocatalyst for the anode and cathode. Note that carbon rod (0.5 cm in diameter) and Ag/AgCl (in 3 M KCl solution) were used as counter and reference electrodes, respectively. Prior to electrochemical measurements, the electrolyte (KOH, 1.0 M, pH = 13.8) were saturated with O₂ for OER and with N₂ for HER. For anodic BA oxidation, the chamber was purged by N₂ to remove O₂ before the addition of BA. Notably, gentle magnetic stirring is necessary to enable a homogeneous distribution of BA in the electrolyte during the anodic oxidation reaction. The Linear sweep voltammetry (LSV) were recorded at the scan rate of 2 mV s⁻¹. The cycling stability test was performed by CV scanning 1000 cycles from 0 to 0.1 V (vs. RHE) at the scan rate of 100 mV s⁻¹.

The overall water splitting and MFHWE measurements. These two experiments were carried out with a two-electrode system without the use of a Nafion membrane.

All potentials ($E_{corrected}$) were corrected with iR (current times internal resistance) compensation to account for the drop in voltage between the reference and working electrodes by eq. 1:

$$E_{corrected} = E_{uncorrected} - iR \quad (1)$$

Faradaic efficiency (FE) for H₂ production was estimated by eq. 2

$$FE = \frac{V_{experimental}}{V_{theoretical}} * 100\% \quad (2)$$

Note that the $V_{experimental}$ is obtained by a water displacement method during the electrochemical measurements. $V_{theoretical}$ is obtained by eq. 3

$$V_{theoretical} = \frac{QV_s}{\alpha F} \quad (3)$$

Where Q is total charge consumed during the water electrolysis or the MFHWE, V_s is the standard molar volume (22.4 L mol⁻¹), α is a constant representing the number of electrons being exchanged in the generation of gas (for H₂ generation, $\alpha = 2$), and F is the Faraday's constant (96485 C mol⁻¹).³

BA conversion during anodic oxidation was evaluated by eq. 4:⁴

$$Conversion_{BA} (\%) = \frac{n_{BA \text{ consumed}}}{n_{BA \text{ added}}} * 100\% \quad (4)$$

The yield of Ph-COOH during anodic oxidation was evaluated by eq. 5:⁴

$$Yield_{Ph-COOH} (\%) = \frac{n_{Ph-COOH \text{ formed}}}{n_{BA \text{ added}}} * 100\% \quad (5)$$

Faradaic efficiency for Ph-COOH production was evaluated by eq. 6:⁵

$$FE_{Ph-COOH \text{ production}} = \frac{n_{Ph-COOH \text{ formed}}}{0.25 * n_{total \text{ electrons passed}}} 100\% \quad (6)$$

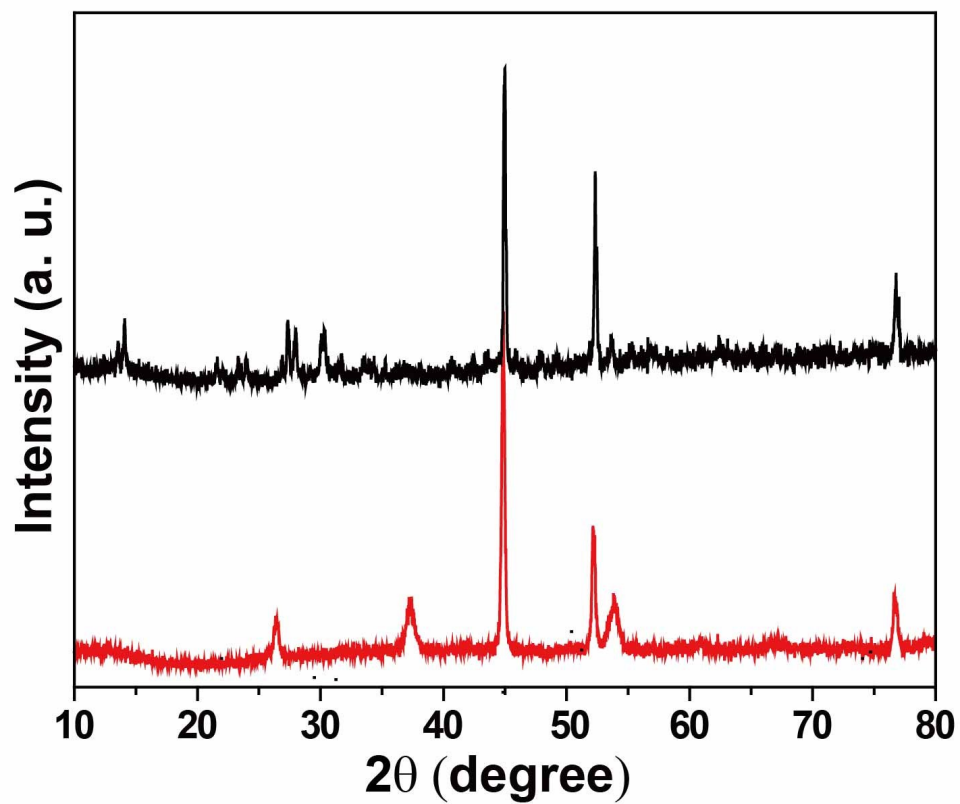


Figure S1. XRD patterns of the hydrothermally produced products before (black curve) and after (red curve) reduction treatment at 500 °C under an atmosphere of H₂/Ar.

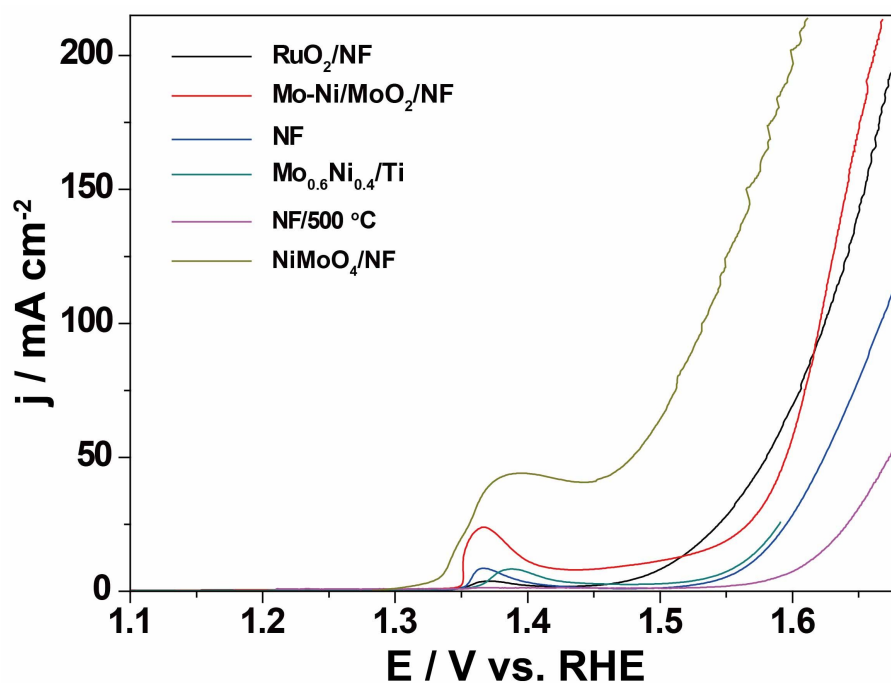


Figure S2. LSV curve comparison of the as-prepared hierarchical Mo-Ni catalyst and other reported (or commercial-available) catalysts, including RuO₂/NF, NF before and after treatment at 500 °C, Mo_{0.6}Ni_{0.4}/Ti and NiMoO₄/NF. The experiments were carried out in an alkaline media (KOH, 1.0 M) at a scan rate of 2 mV s⁻¹.

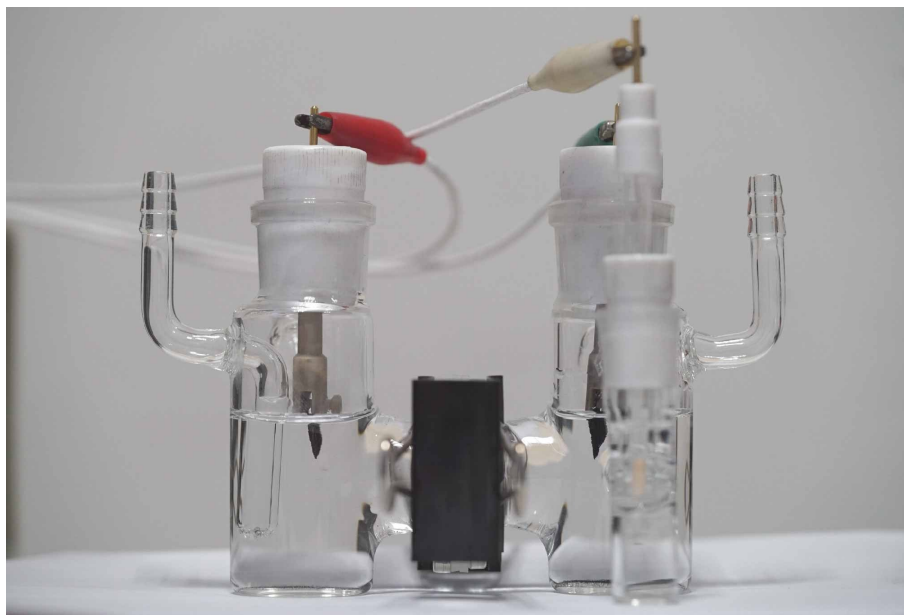


Figure S3. H-type three-compartment cell used for OER, anodic oxidation of BA and HER measurements. Note that the anode and cathode chambers were separated by a Nafion membrane during these experiments.

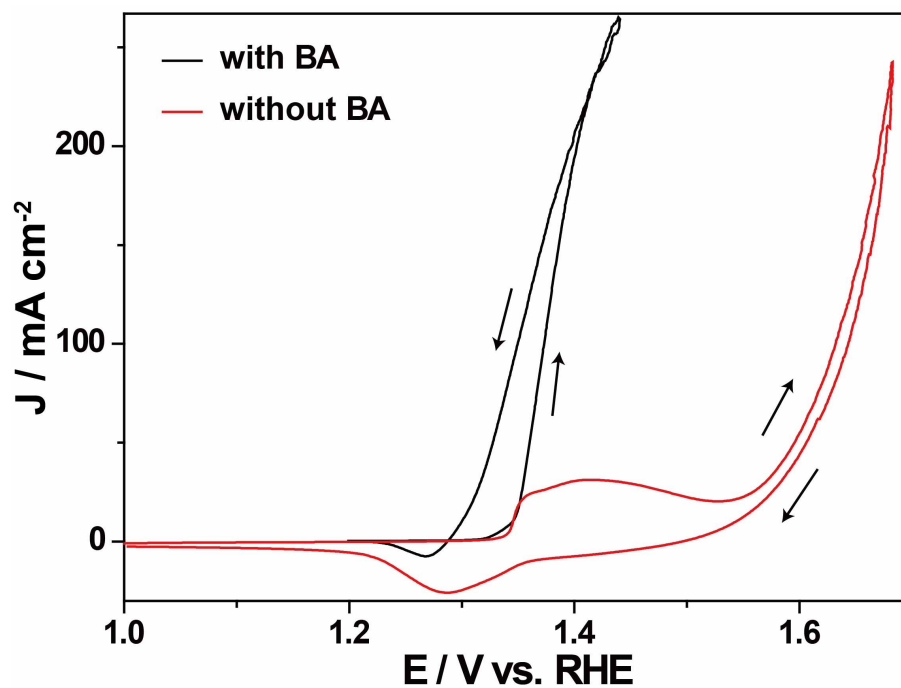


Figure S4. CV profiles of anode of Mo-Ni alloy nanoparticles in 1.0 M KOH in the presence and absence of BA (15 mM). The scanning rate was fixed at 3 mV s⁻¹.

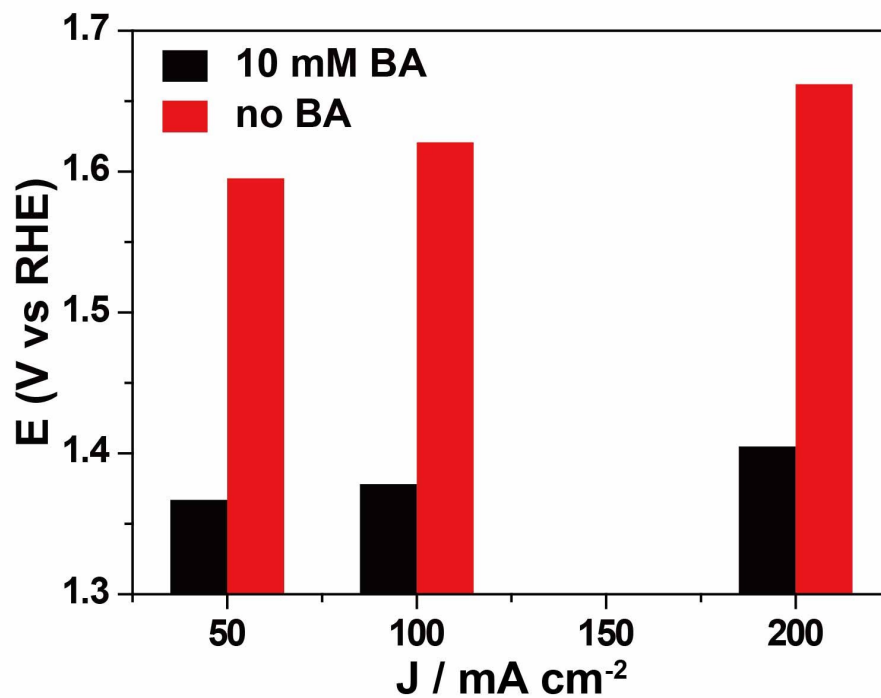


Figure S5. Comparison of potentials at different benchmark current densities of 50, 100 and 200 mA cm^{-2} over the as-prepared Mo-Ni alloy nanoparticle catalyst in KOH (1.0 M) in the presence and absence of BA (10 mM).

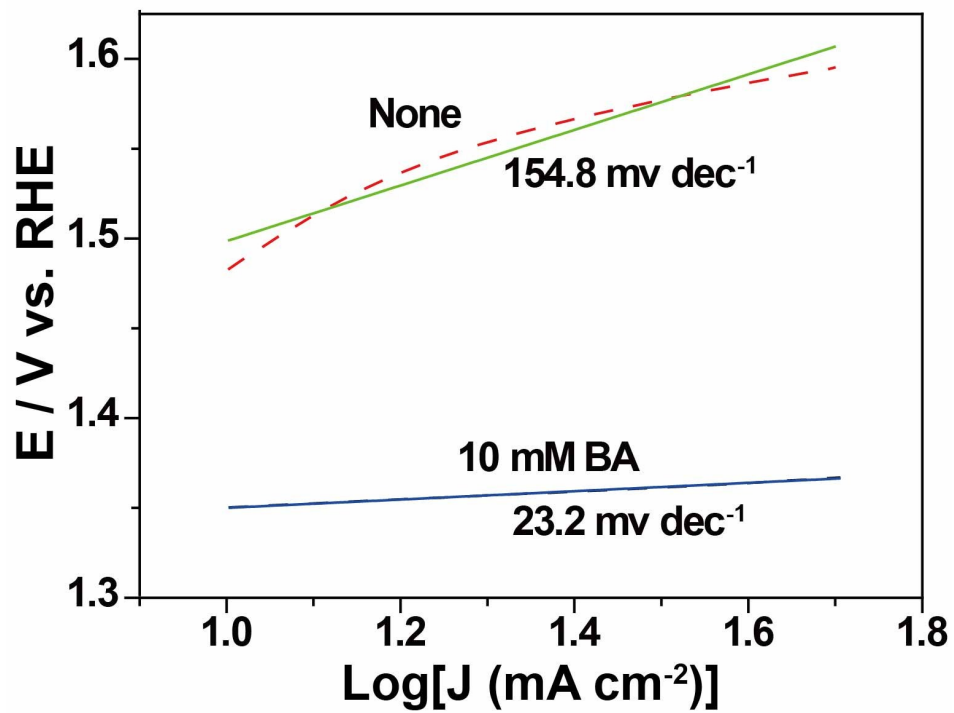


Figure S6. Corresponding Tafel plots for anodic BA oxidation and water oxidation in 1.0 M KOH. Note that the concentration of BA in the anodic chamber is 10 mM.

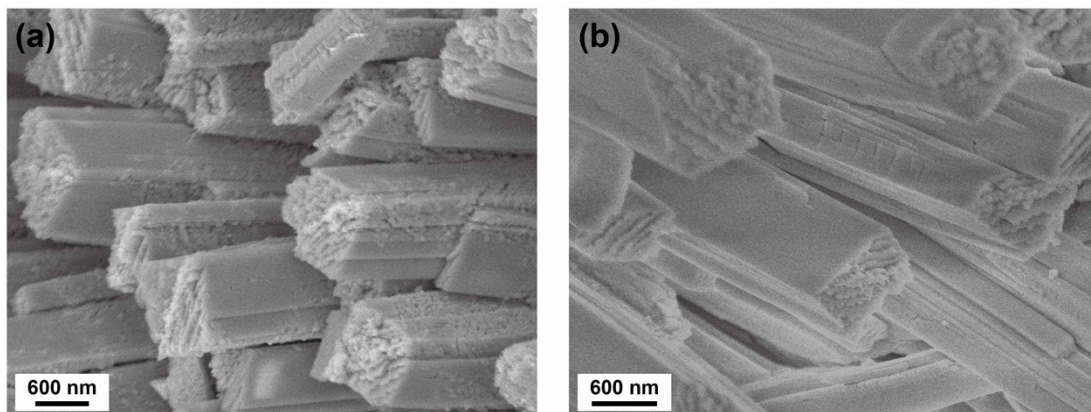


Figure S7. SEM images of Mo-Ni/MoO₂/carbon cloth before and after being etched by H₂SO₄ (2 M).

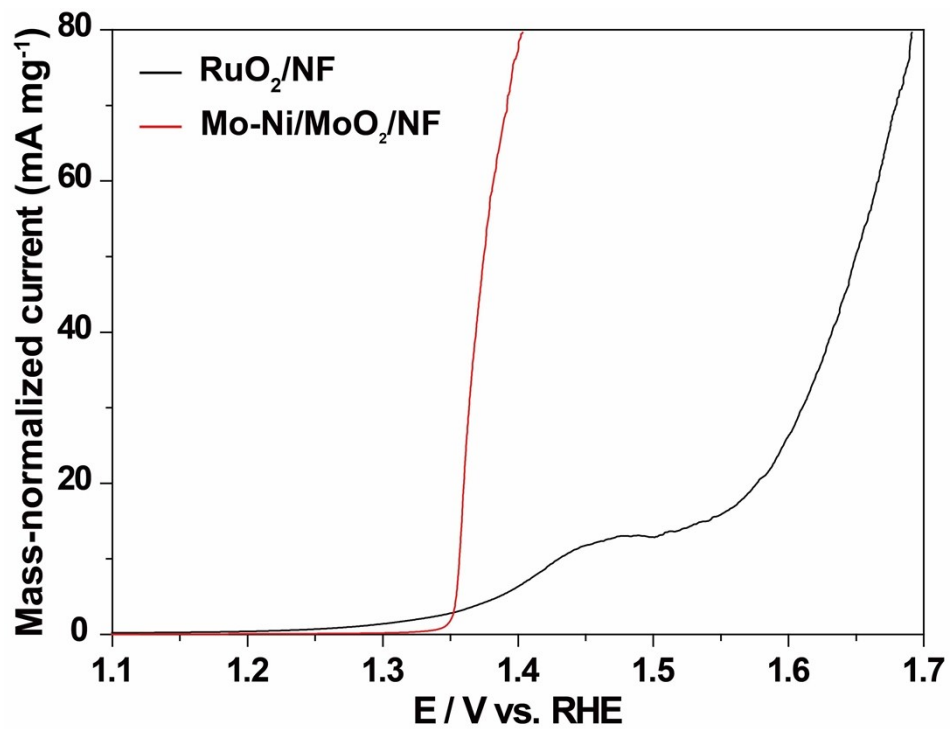


Figure S8. Mass-normalized LSVs of as-prepared Mo-Ni/MoO₂/NF and RuO₂/NF for BA oxidation. The experiments were carried out in 1.0 M KOH at a scan rate of 2 mV s⁻¹.

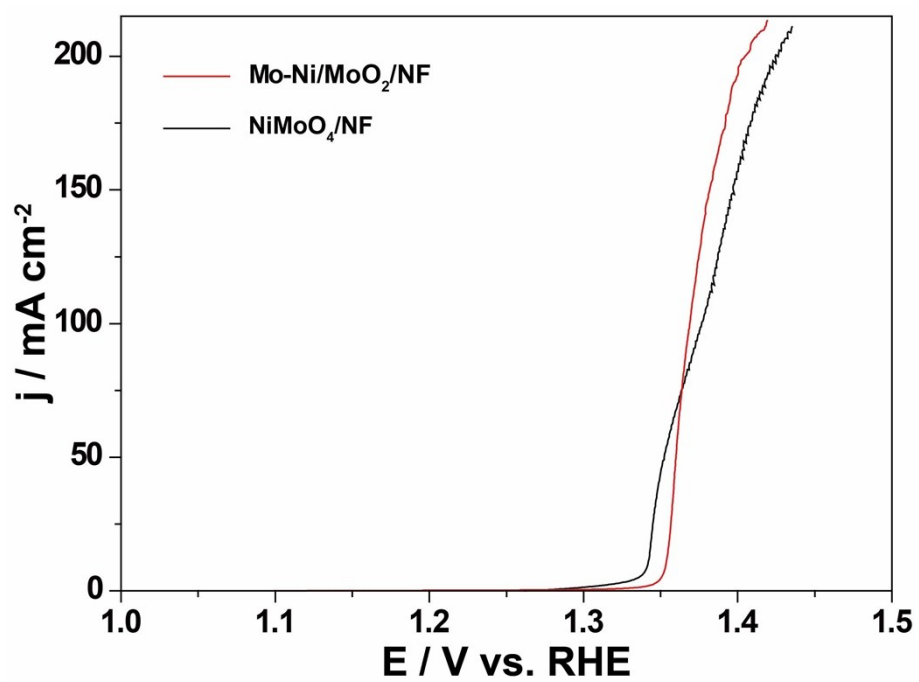


Figure S9. LSV curves of as-prepared Mo-Ni alloy nanoparticles and NiMoO₄ catalyst at a scan rate of 2 mV s⁻¹ in 1.0 M KOH in the presence of BA (10 mM).

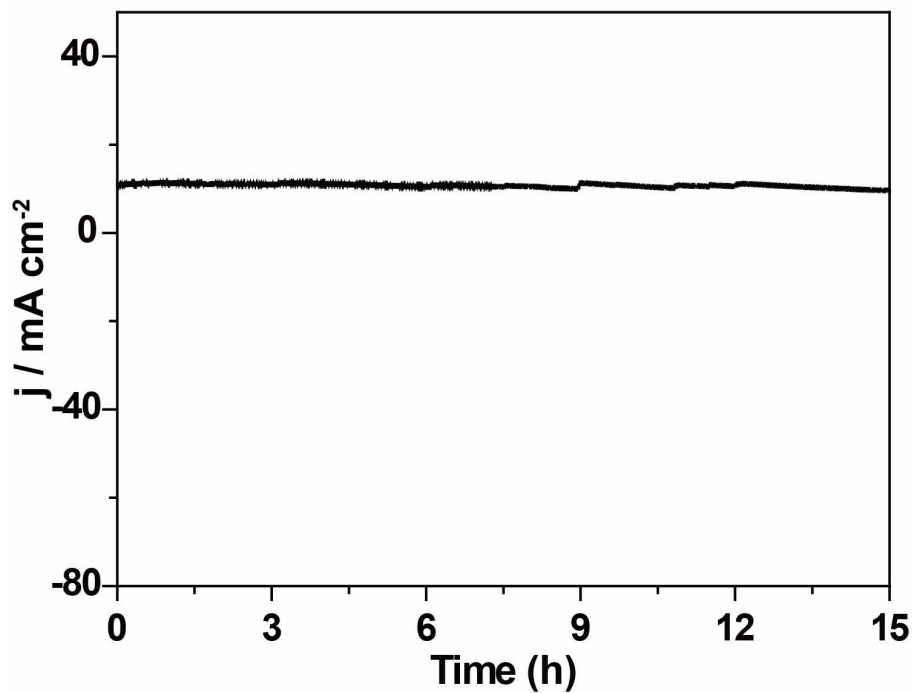


Figure S10. Long-term stability of the as-prepared Mo-Ni alloy nanoparticle catalyst for OER in 1.0 M KOH after the addition of excessive BA (4 mmol). The potential of the experiment was set at 1.34 V (vs. RHE) ($\sim 10 \text{ mA cm}^{-2}$).

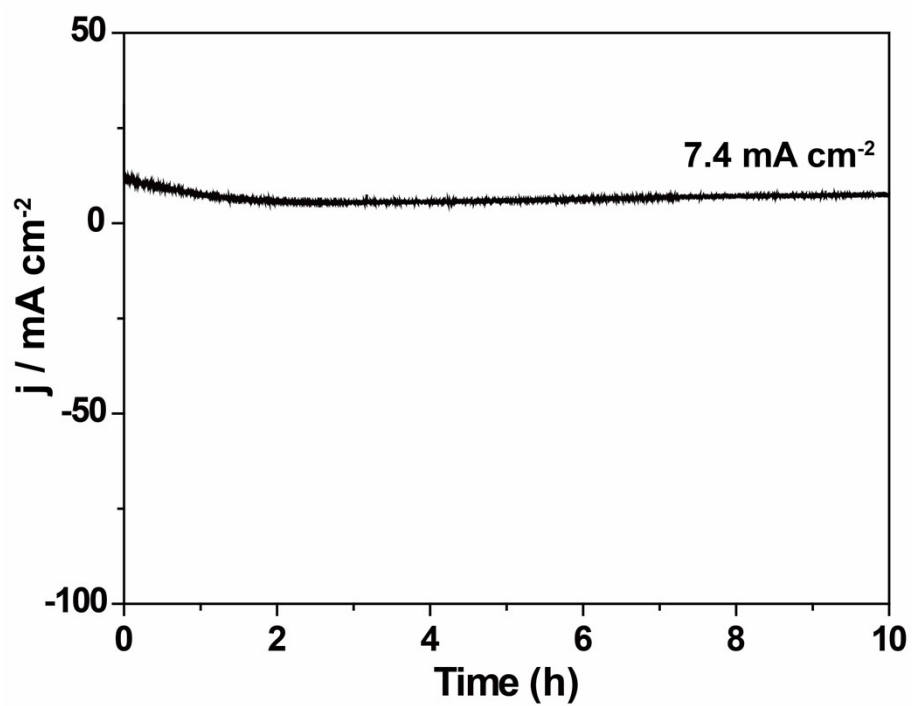


Figure S11. Long-term stability of the as-prepared Mo-Ni alloy nanoparticle catalyst for OER in 1.0 M KOH. The potential was set at 1.5 V (vs. RHE) at yield a current density at 10 mA cm⁻² at the beginning of the experiment.

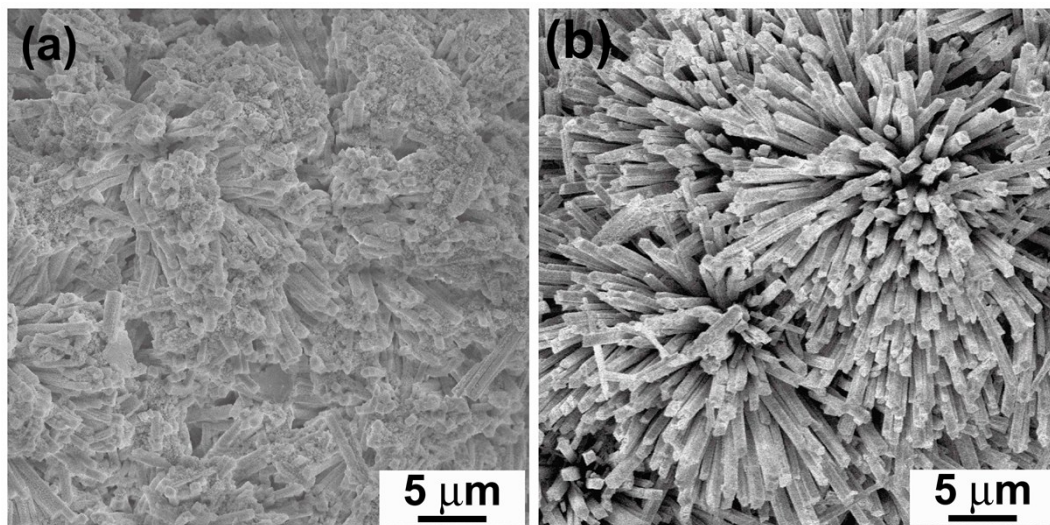


Figure S12. SEM images of the as-prepared Mo-Ni alloy nanoparticle catalyst after water oxidation (a) and BA oxidation (b).

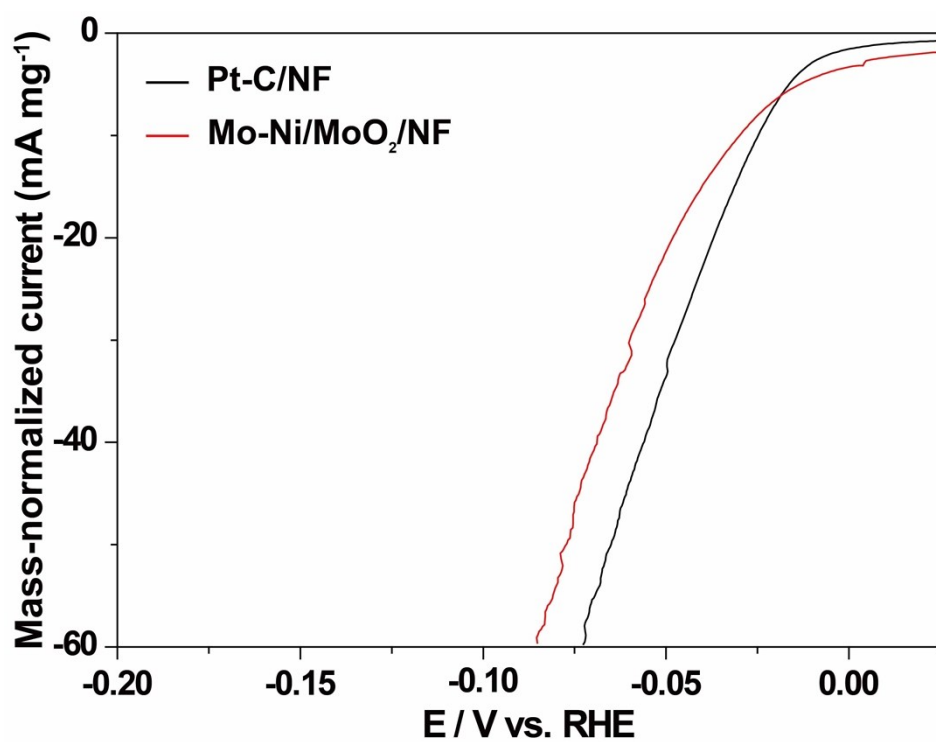


Figure S13. Mass-normalized HER LSVs of as-prepared Mo-Ni/MoO₂/NF and Pt-C/NF. The experiments were carried out in 1.0 M KOH at a scan rate of 2 mV s⁻¹.

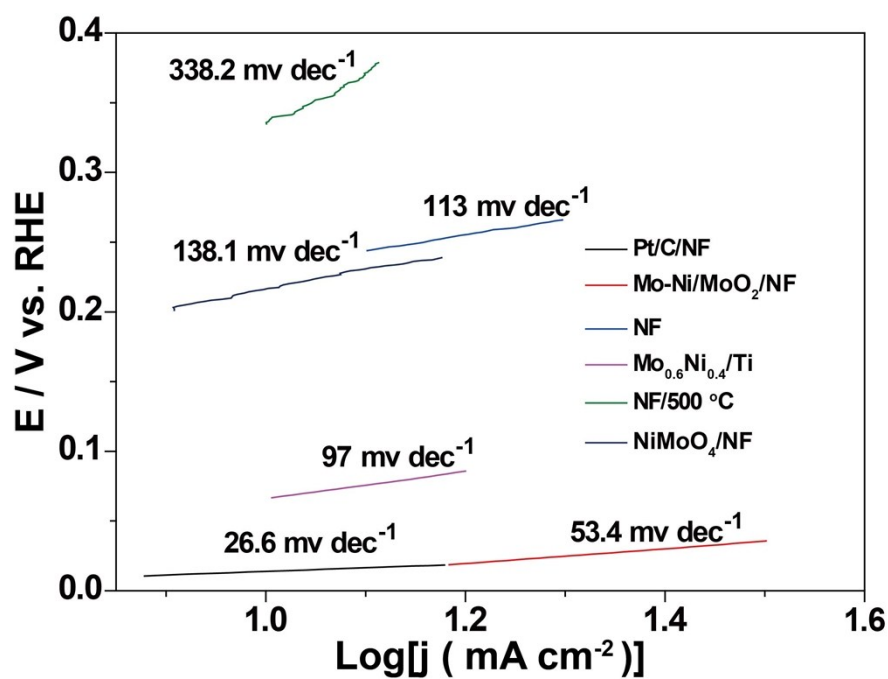


Figure S14. Tafel plot comparison of the as-prepared Mo-Ni alloy nanoparticle catalyst and other reported (or commercial-available) catalysts, including Pt-C/NF, pristine NFs before and after being treated at 500 °C, NiMoO₄/NF, and Mo_{0.6}Ni_{0.4}/Ti.

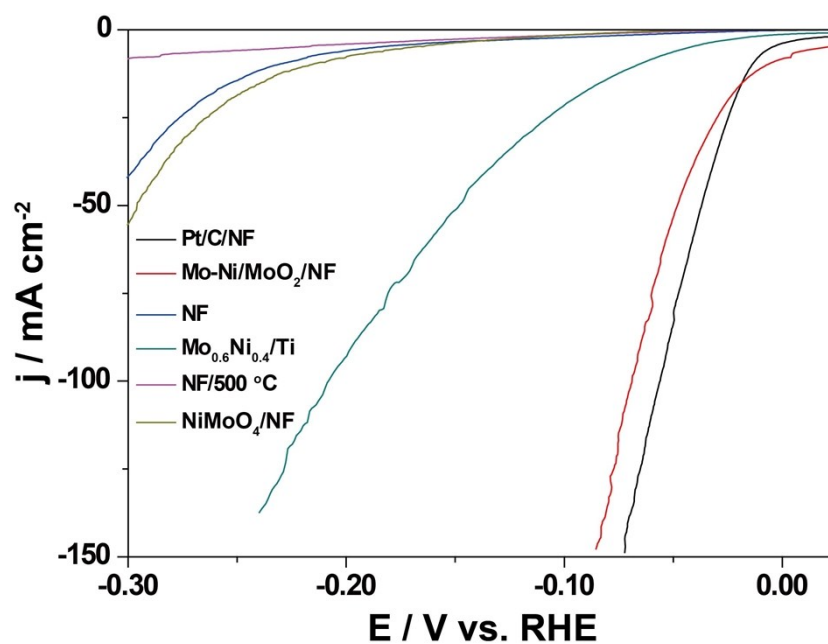


Figure S15. LSV curve comparison of the as-prepared hierarchical Mo-Ni catalyst and other reported (or commercial-available) catalysts, including Pt-C/NF, NiMoO₄/NF, NFs before and after being treated at 500 °C, and Mo_{0.6}Ni_{0.4}/Ti. The experiments were carried out in alkaline media (KOH, 1.0 M) at a scan rate of 2 mV s⁻¹.

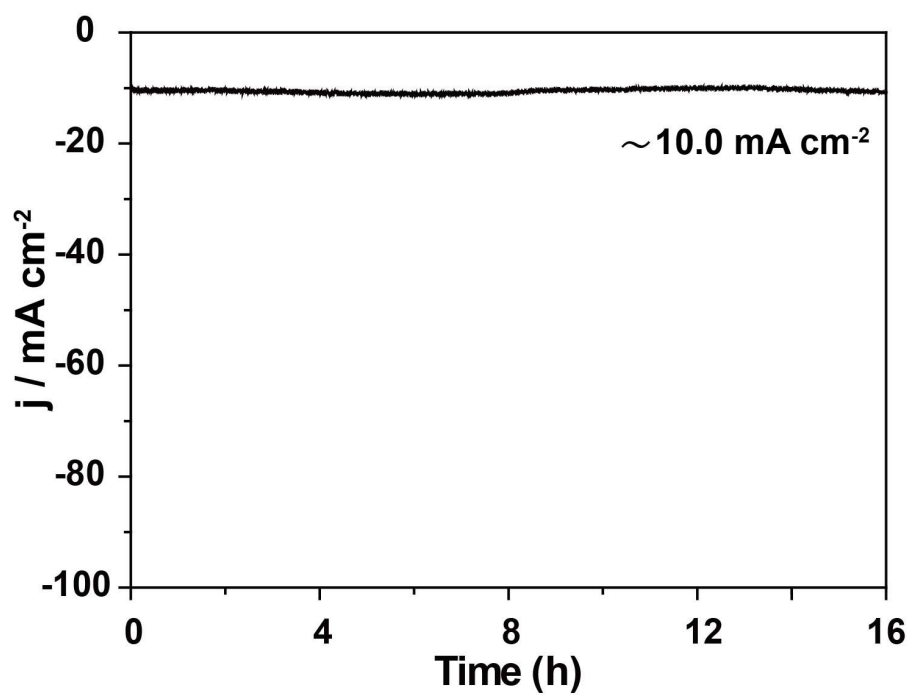


Figure S16. Chronoamperometric curve of the as-prepared Mo-Ni alloy nanoparticle catalyst at an overpotential of 23 mV to yield a current density of 10 mA cm⁻² in 1.0 M KOH.

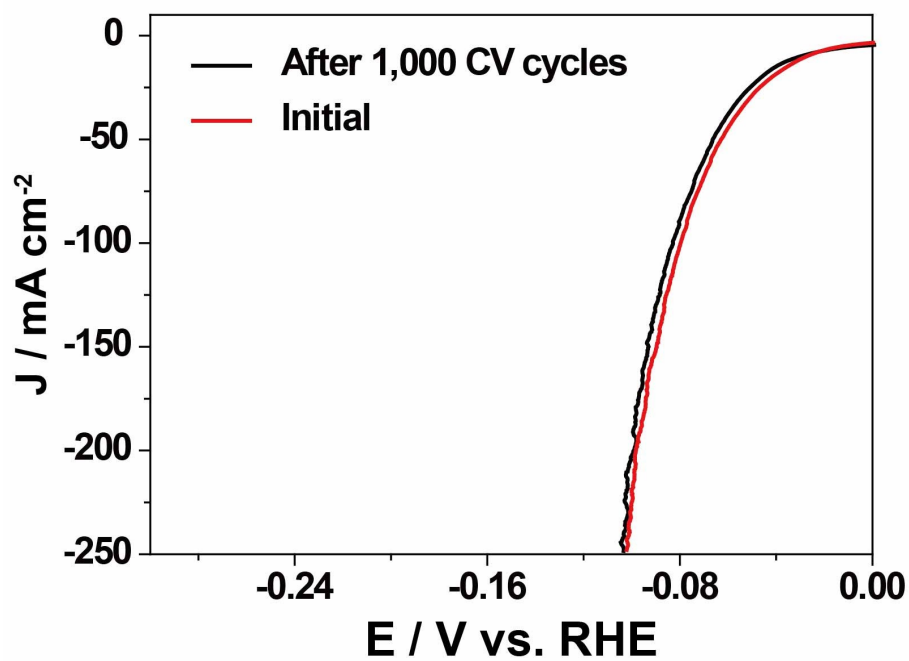


Figure S17. Polarization curves of the as-prepared Mo-Ni alloy nanoparticle catalyst recorded before and after 1000 cyclic voltammograms. Note that all measurements were carried out in 1.0 M KOH.

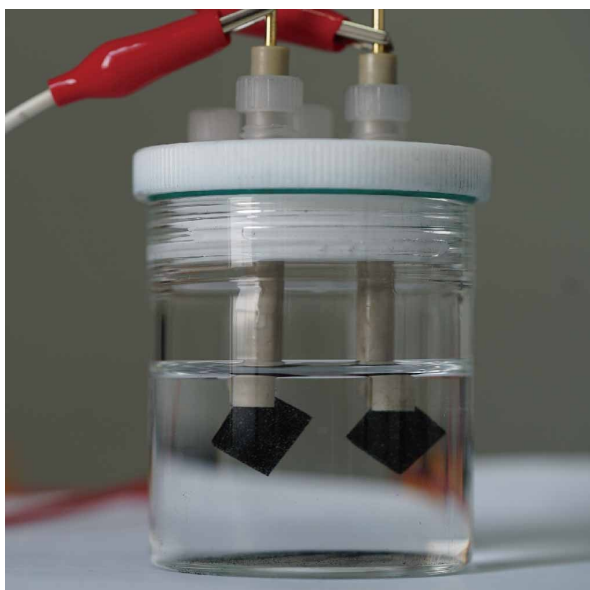


Figure S18. Photograph of the setup used for WFHWE with the use of the as-prepared Mo-Ni alloy nanoparticle catalyst couple in 1.0 M KOH containing BA (10 mM).

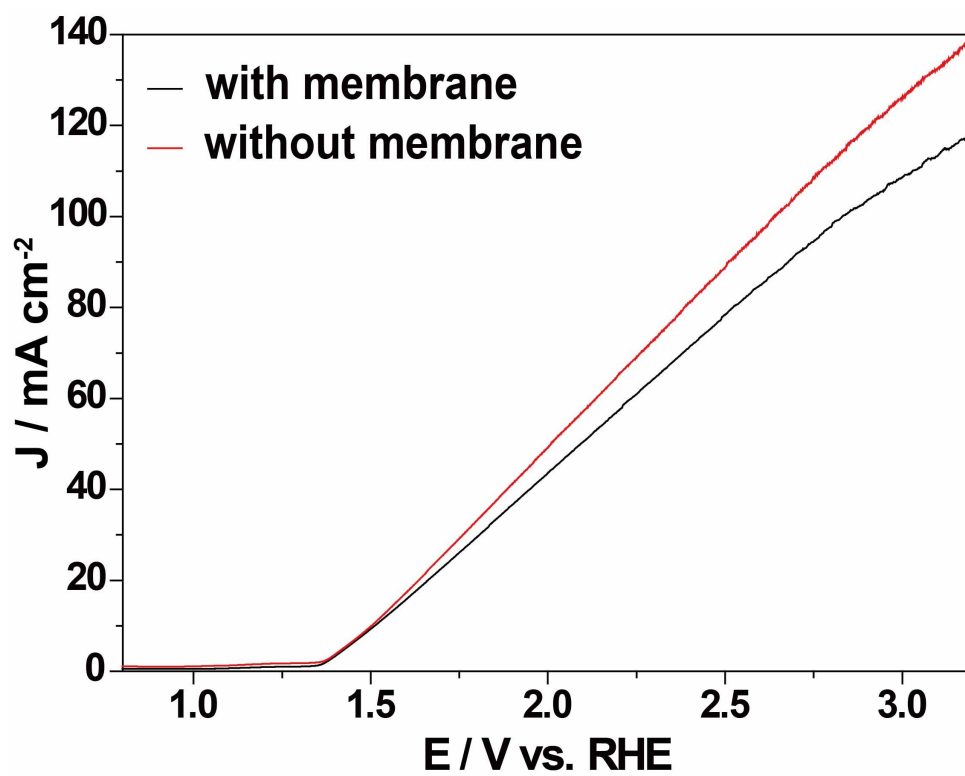


Figure S19. LSV curves for a Mo-Ni nanoparticle catalyst couple with and without use of a Nafion 115 membrane in the electrochemical device. Note that the experiments were carried out in 1.0 M KOH in the presence of BA (10 mM) at a scan rate of 2 mV s⁻¹.

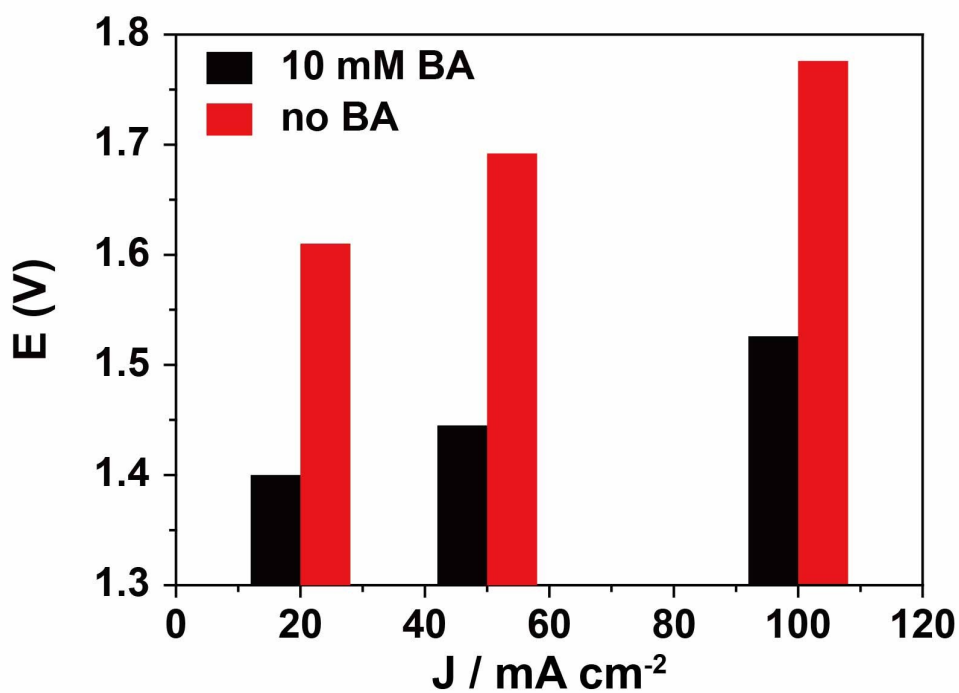


Figure S20. Comparison of the cell voltages to achieve benchmark current densities over as-prepared hierarchical Mo-Ni catalyst couple in 1.0 M KOH with and without BA (10 mM).

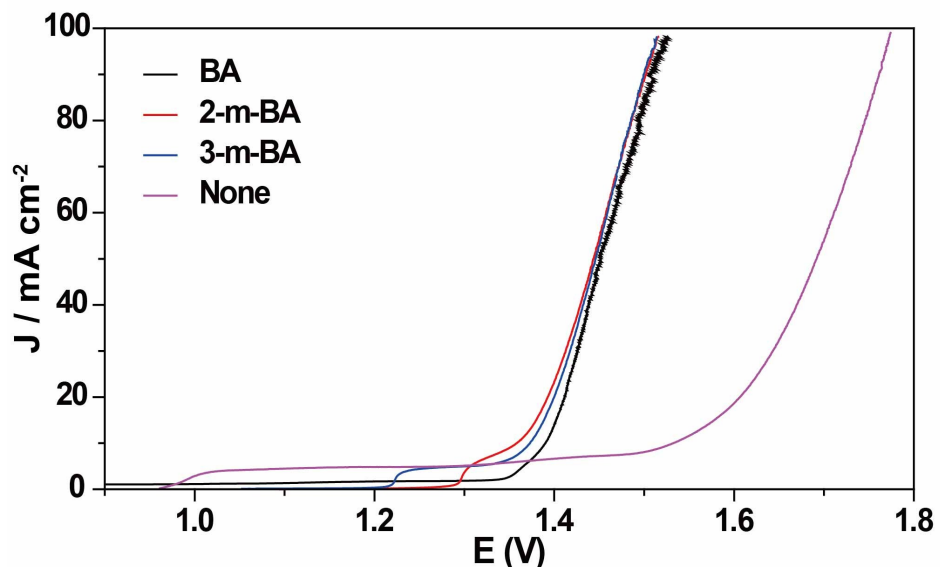


Figure S21. LSV curves of a as-prepared hierarchical Mo-Ni catalyst couple in 1.0 M KOH with and without organic compounds (10 mM).

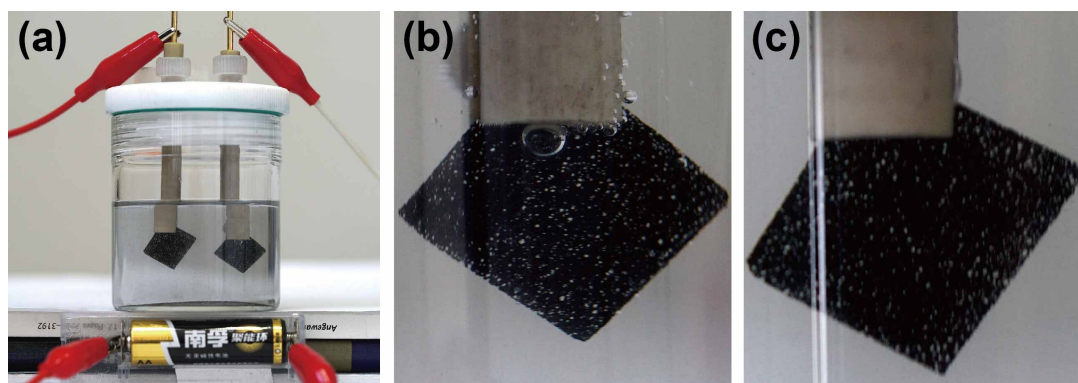


Figure S22. Demonstration of MFHWE in 1.0 M KOH containing BA (10 mM) powered by a single-cell alkaline battery. (a) Photograph of the experimental setup. (b and c) Photographs of the corresponding cathode and anode. It is important to note that there is no gas bubbles on the anode due to the oxidation of BA instead of water.

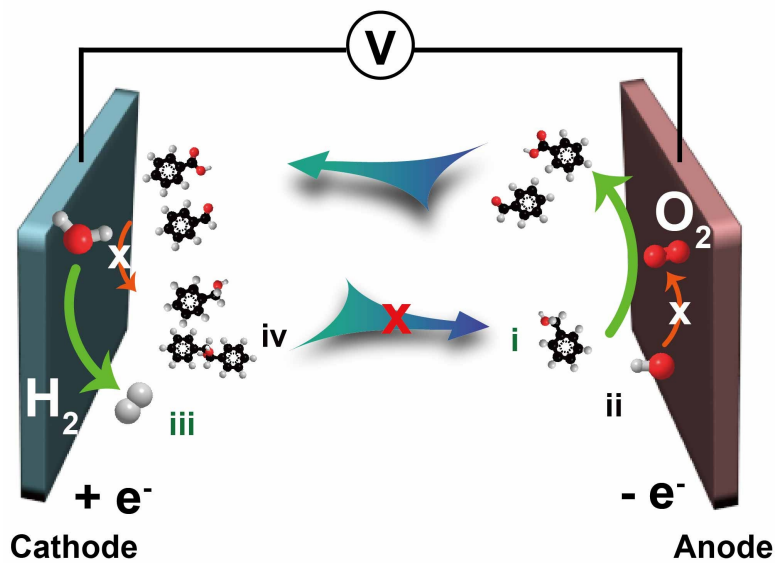


Figure S23. Schematic representation of MFHWE for ultrastable and efficient H_2 production. Note that anodic oxidation of BA is coupled with HER in our strategy. High-performance catalysts for both HER and organic compound oxidation only allows the occurrence of HER and BA oxidation at the cathode and anode, leading to the no need for an ion-conducting membrane to separate the cathodic and anodic reactions.

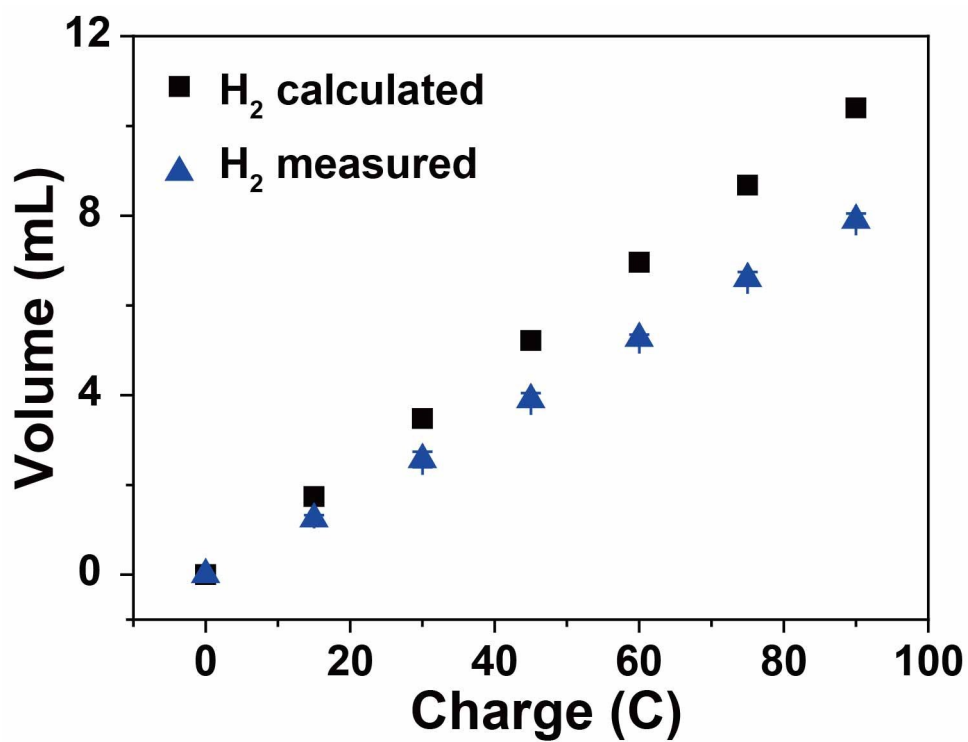


Figure S24. Volume comparison of calculated H₂ and measured H₂ catalyzed by a NF catalyst couple in 1.0 M KOH with the addition of BA (10 mM) and in the absence of a Nafion membrane between the cathode and the anode compartments.

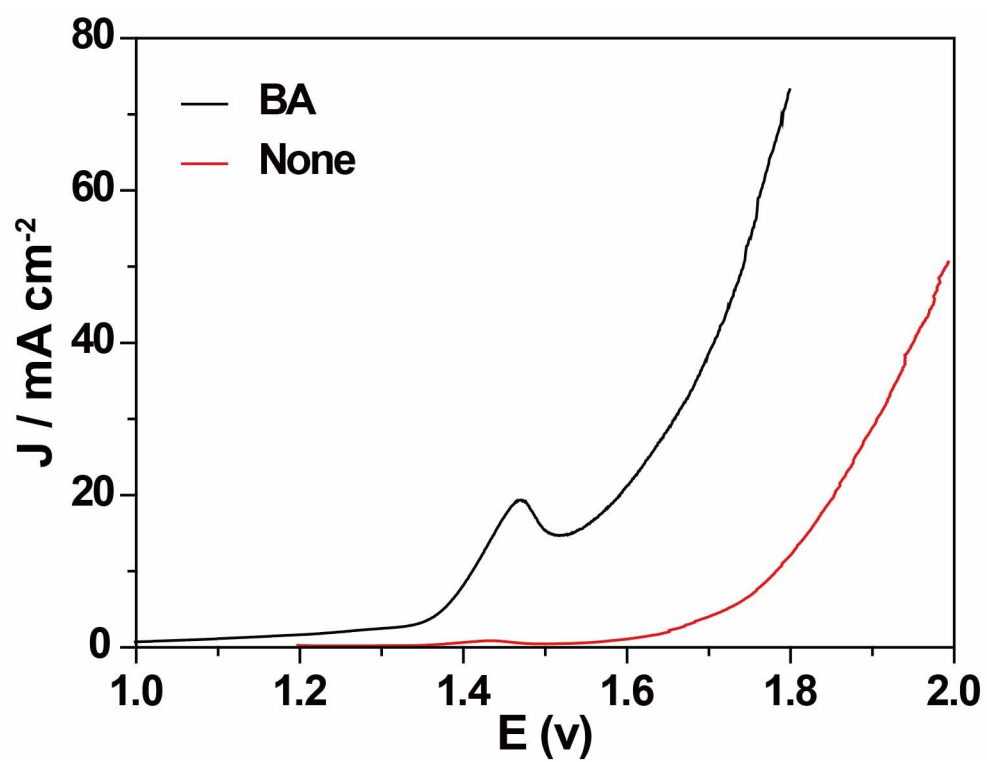


Figure S25. LSV curves of a NF catalyst couple in 1.0 M KOH with and without addition of BA (10 mM).

Table S1. A comparison of the catalytic performance of the as-prepared hierarchical Mo-Ni catalyst with other recently reported catalysts for anodic oxidation of BA.^a

Catalyst	Electrolyte	η_{HER} (V) (vs. RHE)	η_{OER} (V) (vs. RHE)	η^b (V) (vs. RHE)	E_1^c (V)	E_2^d (V)	Refs
Mo-Ni	1 M KOH + 10 mM BA	0.023	1.49	1.345	1.49	1.38	This work
hp-Ni	1 M KOH+ 10 mM BA	0.219 ^e	1.51 (onset)	1.35 (onset)	1.69	1.5	6
Fe/Co200	1 M KOH + 15m M BA	NG	1.54	1.438	1.48	1.42	7
NiCo/AC	1 M KOH + 0.1 M BA	NG	1.57	1.31	1.564	>1.5	8
Co _{0.83} Ni _{0.17} /activated carbon	1 M KOH + 10 mM BA	0.193	1.555	1.425 ^f	1.74	1.54	9
(NC)@CuCo ₂ N _x /carbon fiber	1 M KOH + 15 mM BA	0.105	1.46	1.25 ^g	1.62	1.55	10
<i>h</i> -Ni(OH) ₂ (anode) and PtO ₂ / <i>h</i> -Ni(OH) ₂ (cathode)	1 M KOH + 40 mM BA	NG	NG	NG	1.68	1.48	11

^aUnless stated the potentials were obtained at a current density of 10 mA cm⁻². ^bThe potentials needed for oxidation of BA with a three-electrode configuration. ^cCell voltages required for water electrolysis with a two-electrode configuration. ^dCell voltages required for hybrid water electrolysis (in the presence of BA). ^eAt a current density of 50 mA cm⁻². ^fAt a current density of 30 mA cm⁻². ^gConcentration of BA is 15 M.

References:

- (1) Chen, Y. Y.; Zhang, Y.; Zhang, X.; Tang, T.; Luo, H.; Niu, S.; Dai, Z. H.; Wan, L. J.; Hu, J. S. Self-Templated Fabrication of MoNi₄/MoO_{3-x} Nanorod Arrays with Dual Active Components for Highly Efficient Hydrogen Evolution. *Adv. Mater.* **2017**, 1703311.
- (2) Zhang, J.; Wang, T.; Liu, P.; Liao, Z.; Liu, S.; Zhuang, X.; Chen, M.; Zschech, E.; Feng, X. *Nat. Commun.* **2017**, 8, 15437.
- (3) Zhang, T.; Liu, X.; Cui, X.; Chen, M.; Liu, S.; Geng, B. Colloidal Synthesis of Mo–Ni Alloy Nanoparticles as Bifunctional Electrocatalysts for Efficient Overall Water Splitting. *Adv. Mater. Interfaces* **2018**, 1800359.
- (4) Huang, Y.; Chong, X.; Liu, C.; Liang, Y.; Zhang, B. Boosting Hydrogen Production via Anodic Oxidation of Primary Amines over a NiSe Nanorod Electrode. *Angew. Chem. Int. Ed.* **2018**, 57, 13163.
- (5) Nam, D.H.; Taitt, B.J.; Choi, K. Shin. Copper-Based Catalytic Anodes To Produce 2,5-Furandicarboxylic Acid, a Biomass-Derived Alternative to Terephthalic Acid. *ACS Catal.* **2018**, 8, 1197.
- (6) You, B.; Liu, X.; Liu, X.; Sun, Y. Efficient H₂ Evolution Coupled with Oxidative Refining of Alcohols via A Hierarchically Porous Nickel Bifunctional Electrocatalyst. *ACS Catal.* **2017**, 7, 4564.
- (7) Huang, Y.; Yang, R.; Anandhababu, G.; Xie, J.; Lv, J.; Zhao, X.; Wang, X.; Wu, M.; Li, Q.; Wang, Y. Cobalt/Iron(Oxides) Heterostructures for Efficient Oxygen Evolution and Benzyl Alcohol Oxidation Reactions. *ACS Energy Lett.* **2018**, 3, 1854.
- (8) Liu, G.; Zhao, C.; Wang, G.; Zhang, Y.; Zhang, H. Efficiently electrocatalytic oxidation of benzyl alcohol for energy-saved zinc-air battery using a multifunctional nickel-cobalt alloy electrocatalyst. *J Colloid Interface Sci.* **2018**, 532, 37.
- (9) Liu, G.; Zhang, X.; Zhao, C.; Xiong, Q.; Gong, W.; Wang, G.; Zhang, Y.; Zhang, H.; Zhao, H. Electrocatalytic oxidation of benzyl alcohol for simultaneously promoting H₂ evolution by a Co_{0.83} Ni_{0.17}/activated carbon electrocatalyst. *New J. Chem.* **2018**, 42, 6381.
- (10) Zheng, J.; Chen, X.; Zhong, X.; Li, S.; Liu, T.; Zhuang, G.; Li, X.; Deng, S.; Mei, D.; Wang, J. G. Hierarchical Porous NC@CuCo Nitride Nano sheet Networks: Highly Efficient Bifunctional Electrocatalyst for Overall Water Splitting and Selective Electrooxidation of Benzyl Alcohol. *Adv. Funct. Mater.* **2017**, 27, 1704169.
- (11) Chen, X.; Zhong, X.; Yuan, B.; Li, S.; Gu, Y.; Zhang, Q.; Zhuang, G.; Li, X.; Deng, S.; Wang, J. G. Defect engineering of nickel hydroxide nanosheets by Ostwald ripening for enhanced selective electrocatalytic alcohol oxidation. *Green Chem.* **2019**, 21, 578.